# Effect of Precipitation Sampling Error on Flash Flood Monitoring and Prediction: Anticipating Operational Rapid-Update Polarimetric Weather Radars

YIXIN WEN,[a,b] TERRY SCHUUR,[a,b,c] HUMBERTO VERGARA,[a,b] AND CHARLES KUSTER[a,b]

[a] *Cooperative Institute for Mesoscale Meteorological Studies, University of Oklahoma, Norman, Oklahoma*
[b] *NOAA/National Severe Storms Laboratory, Norman, Oklahoma*
[c] *School of Meteorology, University of Oklahoma, Norman, Oklahoma*

(Manuscript received 13 December 2019, in final form 12 March 2021)

ABSTRACT: Quantitative precipitation estimates (QPE) at high spatiotemporal resolution are essential for flash flood forecasting, especially in urban environments and headwater areas. An accurate quantification of precipitation is directly related to the temporal and spatial sampling of the precipitation system. The advent of phased array radar (PAR) technology, a potential next-generation weather radar, can provide updates that are at least 4–5 times faster than the conventional WSR-88D scanning rate. In this study, data collected by the Norman, Oklahoma (KOUN), WSR-88D radar with ~1-min temporal resolution are used as an approximation of data that a future PAR system could provide to force the Ensemble Framework for Flash Flood Forecasting (EF5) hydrologic model. To assess the effect of errors resulting from temporal and spatial sampling of precipitation on flash flood warnings, KOUN precipitation data (1-km/1-min resolution) are used to generate precipitation products at other spatial/temporal resolutions commonly used in hydrologic models, such as those provided by conventional WSR-88D radar (1 km/5 min), space-based observations (10-km/30-min), and hourly rainfall products (1 km/60 min). The effect of precipitation sampling errors on flash flood warnings are then examined and quantified by using discharge simulated from KOUN (1 km/1 min) as truth to assess simulations conducted using other generated coarser spatial/temporal resolutions of other precipitation products. Our results show that 1) observations with coarse spatial and temporal sampling can cause large errors in quantification of the amount, intensity, and distribution of precipitation; 2) time series of precipitation products show that QPE peak values decrease as the temporal resolution gets coarser; and 3) the effect of precipitation sampling error on flash flood forecasting is large in headwater areas and decrease quickly as drainage area increases.

KEYWORDS: Flood events; Radars/Radar observations; Sampling; Remote sensing; Satellite observations

## 1. Introduction

Flash floods can develop in minutes to hours, cause damage across a large spatial area and create life-threatening conditions, thus posing a unique forecast challenge to National Weather Service (NWS) forecasters. During the 2017 water year alone, floods accounted for $61.4 billion dollars in damage and 137 fatalities in the United States, contributing to a 10-yr (2009–18) average fatality rate that was higher than any other storm-related hazard (https://www.weather.gov/water/). Ashley and Ashley (2008) found that the flash floods accounted for the majority of flood fatalities across the contiguous United States from 1959 to 2005. These studies indicate that improvement in flash flood forecasting is needed to reduce threats to both lives and property (Gourley et al. 2017).

Improved precipitation estimates are essential for accurate flash flood warnings. The high variability of precipitation creates a significant source of uncertainty for hydrologic modeling, especially in steep headwater areas and urban environments where impervious surfaces can become inundated on the order of minutes. Accurate quantification of precipitation is directly related to the temporal and spatial sampling of the observing system. An ideal sensor should be able to capture both temporal and spatial patterns of a precipitation system through its high spatiotemporal sampling. However, in reality, spatiotemporal sampling of observing systems is often limited (Behrangi and Wen 2017). The discrepancy between ideal and actual precipitation measurements is mainly due to technological and financial limitations, hence there are few studies that discuss the variability of precipitation under 5-min resolution.

A variety of precipitation measurements can be used to force hydrologic models. Rain gauges, which hydrologists have traditionally relied upon, provide perhaps the best available point measurements of precipitation; however, they suffer from poor spatial coverage and lack areal representation over land (Kidd et al. 2017). The limited coverage can be problematic for intense rainfall with high spatial variability, which is common for flash flooding. Space-based precipitation measurements are also often used to force hydrologic models due to their complete spatial coverage (Hossain and Anagnostou 2004; Gourley et al. 2011; Maggioni et al. 2013; X. Zhang et al. 2016; Clark et al. 2017). For example, since the spring of 2014, NASA's Global Precipitation Measurement (GPM) mission Integrated Multi-satellite Retrievals for GPM (IMERG; Huffman et al. 2020) has provided gridded precipitation maps with a spatiotemporal resolution of 0.1° × 0.1° (corresponding roughly to a 10-km grid in midlatitude) and 30 min globally (90°N–90°S) within the latitude band 60°N–60°S. The coarse spatiotemporal resolution of IMERG precipitation products, however, may cause sampling errors that can adversely affect hydrologic simulations, especially when monitoring flash

*Corresponding author*: Yixin Wen, berry.wen@noaa.gov

DOI: 10.1175/JHM-D-19-0286.1

floods. In addition, space-based precipitation measurements often have underestimation issues (Wen et al. 2018; Bartsotas et al. 2018). Weather radars provide perhaps the best opportunity to collect precipitation with both high spatial and temporal resolutions. The current NWS Weather Surveillance Radar–1988 Doppler (WSR-88D) network has dramatically increased our ability to observe high-resolution precipitation data in space and time. Technically, WSR-88Ds are capable of implementing scanning strategies that would enable fast scanning with volume update times as low as 1 min. However, the operational WSR-88Ds are still constrained by mechanical scanning to a ~5-min volume update time for data collection in flash flooding events [volume coverage patterns (VCPs) 12 and 212; Federal Coordinator for Meteorological Services and Supporting Research 2013] because the use of those fast scanning strategies is prohibited by constraints designed to ensure that forecasters have adequate upper-level data in precipitation systems and to reduce unnecessary wear and tear on the antenna pedestal (Federal Coordinator for Meteorological Services and Supporting Research 2013). The ground radars also have limitations in complex terrain where they must rely on scans at higher-elevation angles, and thus observations collected from within the ice region of the clouds, to compute QPE at surface. Since the radar beam broadens with range, it also becomes more difficult to accurately resolve the vertical structure of precipitation at long ranges (Wen et al. 2013). In this study, since the primary focus is the examination of hydrologic uncertainties resulting from temporal and spatial resolution instead of uncertainties contributed from instrument calibrations or retrieval algorithms, precipitation measurements of different resolutions will be mimicked from KOUN data to avoid the calibration or algorithm uncertainties.

Research has shown that faster rainfall data update times are desirable for flash flood early warning, especially in small catchments (Berne et al. 2004). Phased array radars (PARs) offer more agile scanning through the use of electronic beam formation and steering (e.g., Zrnic et al. 2007; Heinselman and Torres 2011), collect rainfall data at higher temporal resolutions, and scan the atmosphere and storms adaptively at each azimuth position (Heinselman and Torres 2011), and help to reject the unwanted interference signals by changing the received radiation pattern via adaptive beamforming (Stoica and Moses 2005; Nai et al. 2016). PARs are considered a strong candidate to eventually replace the current WSR-88D network (National Research Council 2002). To demonstrate the benefits provided by phased array technology, the National Severe Storms Laboratory (NSSL), in collaboration with other agencies, has undertaken the development of the first S-band, dual-polarization phased array weather radar [referred to as the Advanced Technology Demonstrator (ATD)]. However, since the ATD is not yet ready for operational use, there is a current need for rapid-update datasets that can be used to assess the benefits of phased array technology. To address this need, in the spring of 2013, NSSL conducted the Rapid-Scan Polarization Experiment (RSPE; Burgess et al. 2014), in which the scan strategy of the polarimetric KOUN WSR-88D research radar (located in Norman, Oklahoma) was modified to collect rapid (~1-min volume), sectorized observations when requested. Since then, KOUN has been collecting data to serve as an approximation for those collected by future PARs (Tanamachi and Heinselman 2016). This study is the first to use single operational radar observations to quantify the variability of precipitation at unprecedented high spatiotemporal resolution and examine its impact on hydrologic simulations. In this paper, we use two of those datasets to examine the potential benefits provided by high temporal and spatial resolution data for the modeling of flash floods.

Past studies have discussed the sensitivity of streamflow simulation in urban catchments to the X-band radar spatiotemporal resolution of precipitation input (Rafieeinasab et al. 2015) and have evaluated the advantages of using X-band polarimetric radar to improve hydrological application at hourly resolution in eastern Italian Alps (Anagnostou et al. 2018). The smaller radar systems, such as X-band radar systems, may have faster updates than the operational S-band tradition radars. However, the X-band systems, due to their well-known severe attenuation issues, are not under consideration as potential replacement for the S-band WSR-88 operational radar network. S-band PAR radars, on the other hand, have been actively studied (Weber et al. 2007; Zrnic et al. 2007) and are recognized as a potential replacement candidate for the current operational WSR-88D network across the United States. The potential of an S-band PAR, rather than radars that operate at other frequencies, to improve flash flood warning provides the motivation for this study. The goal of this study is to leverage the high resolution of rapid-update KOUN observations to further quantify the uncertainties in hydrologic modeling of flash floods contributed by high rainfall variability, which is poorly sampled at low temporal and spatial resolutions. In doing so, the following questions are addressed: Do the 1-min data collected by rapid-update S-band radars improve the detection of flash floods? If so, what catchment size would benefit most from high-resolution precipitation measurements? How large are the flash flood simulation errors resulting from temporal and spatial precipitation samplings when compared with simulations from the 1-min KOUN data? These questions will be answered in the following sections of this paper. In section 2 we describe the rainfall datasets and the hydrological model used in the study. Section 3 presents differences among rainfall products of different spatiotemporal resolutions. Section 4 investigates the performance of discharge simulations from different rainfall datasets, and concluding remarks are presented in section 5.

## 2. Hydrological model and rainfall dataset

### *a. Ensemble Framework for Flash Flood Forecasting*

The Ensemble Framework for Flash Flood Forecasting (EF5) is an open-source framework that encompasses the processes for flash flood modeling (Flamig et al. 2020). The EF5 is the hydrologic modeling engine central to the Flooded Locations and Simulated Hydrographs (FLASH) project, which is designed

and optimized to improve NWS forecasters' ability to monitor and forecast flash flooding (Gourley et al. 2017). The parameterization of EF5's water balance models using geospatial datasets is described by Clark et al. (2017). Vergara et al. (2016) describes a regionalization technique to estimate the routing parameters in the model channels, which results in a priori estimates for routing parameters at all grid cells across the continental United States (CONUS).

The EF5 products include soil saturation (%), discharge ($m^3 s^{-1}$), and discharge normalized by the cell's upstream drainage area (referred to as unit discharge; $m^3 s^{-1} km^{-2}$). The unit discharge product is most directly applicable to flash flood forecasting. The normalization of discharge by basin area helps to focus the products on those specific locations that are most likely experiencing anomalous flows, rather than merely identifying large discharges that occur regularly in major river systems. In general, a peak unit discharge of $1.5 m^3 s^{-1} km^{-2}$ is typically used as one of the flash flood quick reference guides by NWS forecasters (Martinaitis et al. 2017). The accuracy of peak unit discharge is important in operational flash flood monitoring. A robust, statistically sound evaluation using a decade-long archive of Multi-Radar Multi-Sensor (MRMS; J. Zhang et al. 2016) radar-only precipitation rates at 1-km/5-min resolution against 1643 USGS-gauged basins showed that peak flows simulated by EF5 correlate well with observed discharges as indicated by a Pearson (linear) correlation of 0.64 and Spearman (rank) correlation of 0.79 (Gourley et al. 2017). The EF5 model in the FLASH system with a priori parameters requires no discharge-based calibration and is a robust tool to conduct the rainfall resolution test in this study.

The EF5 model is designed to enable multiscale hydrological simulations ranging from coarse scale (grid size of tens of kilometers) to fine resolution (grid size of 1 km or less). The update frequency of the EF5 model may be varied, as frequently as 1-min intervals. To warm up the model states, a minimum 6-month simulation period is needed. In this study, all QPE products (KOUN, simWSR88D, simIMERG, and simHourly) are generated on the same 1 km × 1 km grid as the digital elevation model resolution and the model update frequency is consistent with each precipitation product's temporal resolution. Since KOUN is an event-based research radar and hence has no continuous precipitation observations, MRMS radar-only precipitation rates were used to warm up the model states.

### b. *Rapid-update polarimetric KOUN observations*

In this paper, we focus on observations collected by the polarimetric WSR-88D (KOUN; Fig. 1) in Norman, Oklahoma. KOUN served as the prototype polarimetric radar that was used to demonstrate the operational advantages of polarimetric observations during the Joint Polarization Experiment (JPOLE; Ryzhkov et al. 2005b). Validation of the polarimetric KOUN radar rainfall estimation in previous studies yielded very positive results, confirming the high quality of the polarimetric radar data (Ryzhkov et al. 2005a; Giangrande and Ryzhkov 2008). After JPOLE, NSSL engineers modified the KOUN antenna control system software to allow for on-demand,

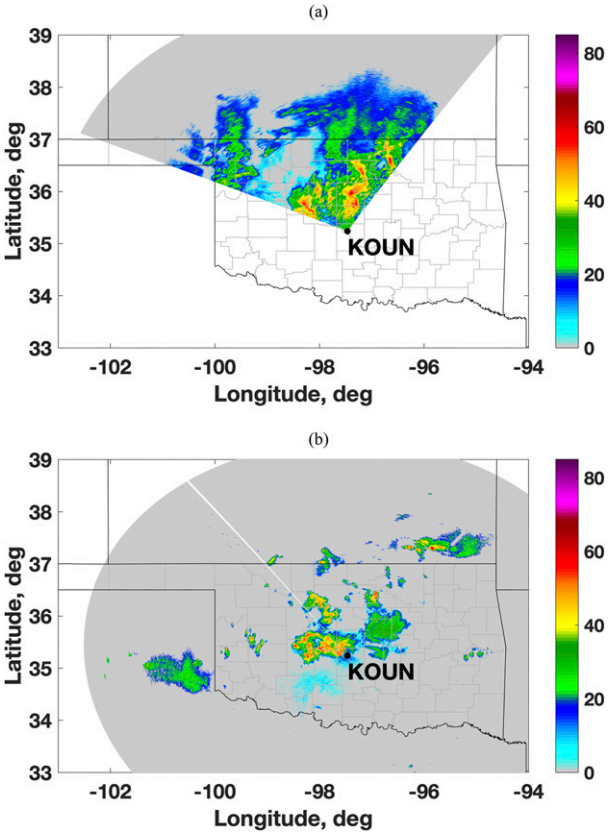


FIG. 1. KOUN rapid-scan VCPs: (a) reflectivity data are collected over a 90° sector with 0.5° azimuthal spacing and 250-m range resolution, with four elevation angles (0.5°, 1.0°, 1.6°, and 2.4°) at 0754:59 UTC 29 Apr 2017 and (b) reflectivity data are collected over 360° with 0.5° azimuthal spacing and 250-m range resolution, with two elevation angels (0.5°, 1.0°) at 0054:57 UTC 14 Aug 2018.

customized, and sectorized scanning. These modifications enable volume update times from 1 min to a few minutes, thereby making it possible to emulate the rapid-update capabilities of polarimetric PARs. Two scanning strategies were adopted to observe the flash flood events that are presented in this study. The first included four elevation angles (0.5°, 1.0°, 1.6°, and 2.4°) that were sampled over a 90° sector with a volume update time of ~37–38 s. This strategy was used to collect rapid-update observations from 0353 to 1308 UTC of the 29 April 2017 central Oklahoma flash flood event (Fig. 1a). The second included two elevation angles (0.5° and 1.0°) that were collected over all 360° in azimuth with a volume update time of ~1 min. This strategy was used to collect rapid-update observations from 2037 to 0900 UTC of the 14–15 August 2018 central Oklahoma flash flood event (Fig. 1b). The 0.5° elevation angle for this event was used to estimate rainfall rates at the surface, and the 1.0° elevation angle was used only if there was excessive ground clutter on the 0.5° elevation angle data. Both scanning strategies employ data oversampling to achieve 0.5° azimuthal spacing, known as "super resolution" (Brown et al. 2002). Since the update times of both events are about

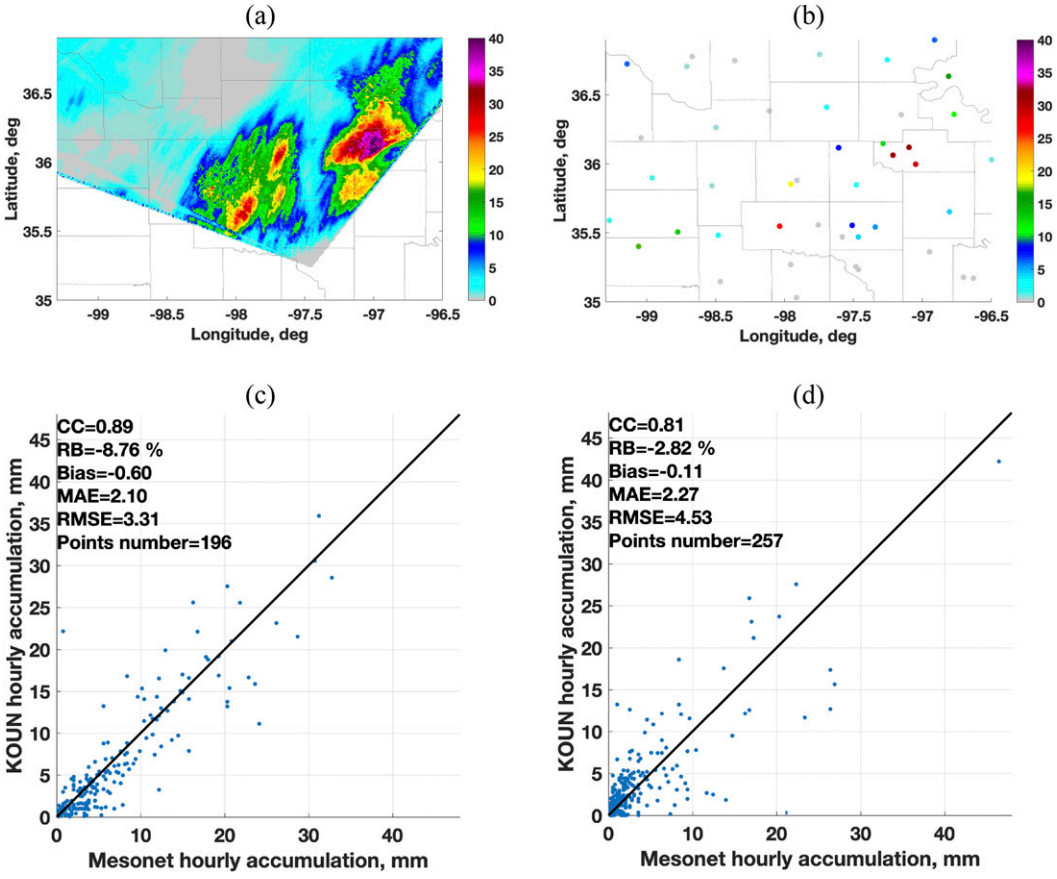


FIG. 2. Hourly accumulation from 0800 to 0900 UTC 29 Apr 2017 derived from (a) polarimetric KOUN data and (b) Mesonet rain gauge observations. The color bars represent accumulations (mm). Hourly radar-gauge rainfall accumulation scatterplots for (c) 29 Apr 2017 and (d) 15 Aug 2018 are also included.

1 min or less, KOUN data used as input for hydrologic simulations in this study was fixed at 1 min by selecting KOUN measurements at the closest time. Since the update times of both events are about 1 min or less, KOUN data used as input for hydrologic simulations in this study were fixed at 1 min by selecting KOUN measurements at the closest time. With this methodology, we understand that we were neglecting temporal variability on the order of a few seconds, but we consider them to be unimportant and will not change the final conclusions. Note that operational WSR-88Ds have a dynamic scanning option called Multiple Elevation Scan Option for Supplemental Adaptive Intravolume Low-Level Scan (MESO-SAILS; Chrisman 2014). When active, anywhere from one to three supplemental low-level scans can be added to any volume, increasing overall low-level data availability to every 75–90 s. Even though higher temporal resolution datasets have already been collected by WSR-88Ds using MESO-SAILS in the past, the hydrologic benefits using this data have still never been demonstrated.

Improvement of QPE is one of the primary benefits of polarimetric radars. Polarimetric radars can improve QPE through the identification and removal of nonmeteorological echoes, classifying hydrometeors, estimating drop size distributions, and correcting attenuation in precipitation (Ryzhkov and Zrnic 2019). In this study, the quality-controlled polarimetric variables collected at 0.5° elevation were used to compute rainfall rates using the QPE algorithm described by Giangrande and Ryzhkov (2008), wherein the polarimetric rainfall algorithm used is determined by an a priori determination of hydrometeor type by a hydrometeor classification algorithm (HCA; Park et al. 2009). Following the HCA, QPE is computed using a $R(Z, Z_{DR})$ relation in areas classified as pure rain, and a $R(K_{DP})$ relation in areas classified as a rain and hail mixture. The $R(Z)$ relations with various intercept parameters determined empirically from comparisons with gauges were used for different types of frozen hydrometeors. An example of hourly radar rainfall accumulation from 0800 to 0900 UTC 29 April 2017 using this synthetic polarimetric radar QPE method is shown in Fig. 2a. In this study, Oklahoma Mesonet gauge (Van der Veer Martens et al. 2017) accumulations are used to validate the polarimetric QPE product. The hourly rainfall accumulation observed by Oklahoma Mesonet gauges from the same time is shown in Fig. 2b. We compare hourly gauge and radar rainfall accumulations over gauge locations. Scatterplots and statistics of comparing KOUN hourly precipitation accumulations to collocated rain gauge accumulations for the two

events are shown in Figs. 2c and 2d, indicating good performance of the computed KOUN polarimetric QPE. For KOUN, the along-radial resolution of the gates is 250 m, and the beam diameters of WSR-88D for beamwidths of 0.93° at range of 50 and 100 km are 0.81 and 1.62 km, respectively (Wood and Brown 1997). The precipitation fields from the KOUN polarimetric QPE algorithm were then interpolated linearly from the spherical coordinate system (azimuth and range) into the Cartesian coordinate system centered at KOUN with a horizontal resolution of 1 km to match spatial resolution of EF5 model in current FLASH system.

### c. Rainfall data with different resolutions

In this study, QPE products with four different resolutions are used to simulate the discharges. Since the primary focus of this study is the examination of hydrologic uncertainties resulting from temporal and spatial resolution instead of uncertainties contributed from instrument calibrations or retrieval algorithms, the other three precipitation products with coarser resolutions are simulated from 1-km/1-min KOUN observations. The three simulated QPE products with coarser resolutions represent three QPE products: 1) 1-km/5-min rainfall representing the WSR-88D radar observations, 2) 10-km/30-min rainfall representing NASA GPM/IMERG products (Huffman et al. 2020), and 3) 1-km/60-min rainfall to focus on the hydrologic effect of hourly temporal resolution that is commonly used by the hydrology community (Gourley et al. 2011). The hydrologic simulations using KOUN rainfall rates are then used as the benchmark to evaluate the hydrologic simulations forced by other precipitation products of different temporal and spatial resolutions. The WSR-88Ds are constrained by mechanical scanning to ~5-min volume update time when 14 elevation angles are used, as in VCPs currently implemented for data collection in convective storms (VCPs 12 and 212; Federal Coordinator for Meteorological Services and Supporting Research 2013). Since radar and satellite are taking instantaneous "snapshot" measurement, the KOUN 1-km/1-min rainfall field was selected every fifth time step to mimic the WSR-88D 1-km/5-min resolution. To mimic the IMERG 10-km/30-min rainfall, the KOUN 1-km/1-min rainfall field was selected every 30th time step with the rainfall remapped to a 10-km grid using the triangulation-based linear interpolation. For the 1-km/60-min rainfall, the KOUN 1-km/1-min rainfall field was simply selected every 60th time step. A similar method to test the effect of resolution of satellite QPEs on hydrologic simulations was adopted in Vergara et al. (2014). The four rainfall products are listed in Table 1 and are hereafter referred to as KOUN, simWSR88D, simIMERG, and simHourly. Note that the simIMERG only addresses the sampling interval and spatial resolution provided by IMERG. The actual IMERG would bring additional errors from the 3-h observation interval for satellite data, algorithm errors, and smoothing in the morphing process.

### d. Verification statistics

The two primary goals that we seek to address in this study are the ability of each precipitation product to 1) detect flash flooding and 2) accurately quantify the simulated discharge.

TABLE 1. A summary of rainfall products tested in this study.

| QPE products | Spatial resolution (km) | Temporal resolution (min) |
|---|---|---|
| KOUN | 1 | 1 |
| simWSR88D | 1 | 5 |
| simIMERG | 10 | 30 |
| simHourly | 1 | 60 |

Simple contingency table statistics are applied to answer the first question. In this study, grid points that have a peak unit discharge greater than 1.5 $m^3 s^{-1} km^{-2}$, as simulated using the KOUN 1-km/1-min precipitation product, are defined as flash flood area. Contingency table statistics describing the probability of detection (POD), false alarm ratio (FAR), and critical success index (CSI) are then used to evaluate flash flooding forecasts that are produced by the other precipitation products. These indices are computed based on the number of hits $H$, false alarms $F$, and misses $M$:

$$\mathrm{POD} = H/(H + M), \tag{1a}$$

$$\mathrm{CSI} = H/(H + F + M), \tag{1b}$$

$$\mathrm{FAR} = F/(H + F). \tag{1c}$$

To answer the second question, three statistical indices for evaluating the simulated discharge are selected. The relative bias (RB) is used to assess the systematic bias of simulations. The mean absolute error (MAE) measures the average magnitude of the error while the root-mean-square error (RMSE) applies more weight to larger errors:

$$\mathrm{RB} = \frac{\sum P(i) - \sum K(i)}{\sum K(i)} \times 100\%, \tag{2a}$$

$$\mathrm{MAE} = \frac{\sum |P(i) - K(i)|}{N}, \tag{2b}$$

$$\mathrm{RMSE} = \sqrt{\frac{\sum [P(i) - K(i)]^2}{N}}. \tag{2c}$$

Here, $P(i)$ and $K(i)$ represent the peak unit discharge simulated by each of the coarse resolution precipitation products and the peak unit discharge simulated by KOUN for the $i$th grid point, respectively, and $N$ represents the total number of grid points. Since the three indices are focused on quantitative measurement rather than detection, only data pairs with nonzero values from simulations are considered.

### e. Overall experimental design

We summarize our procedure to assess the impact of the precipitation sampling error on flash flooding forecasts with the following steps:

- The EF5 hydrologic modeling framework is used to simulate the discharge and unit discharge.
- MRMS radar-only precipitation rates are used to warm up the model states.

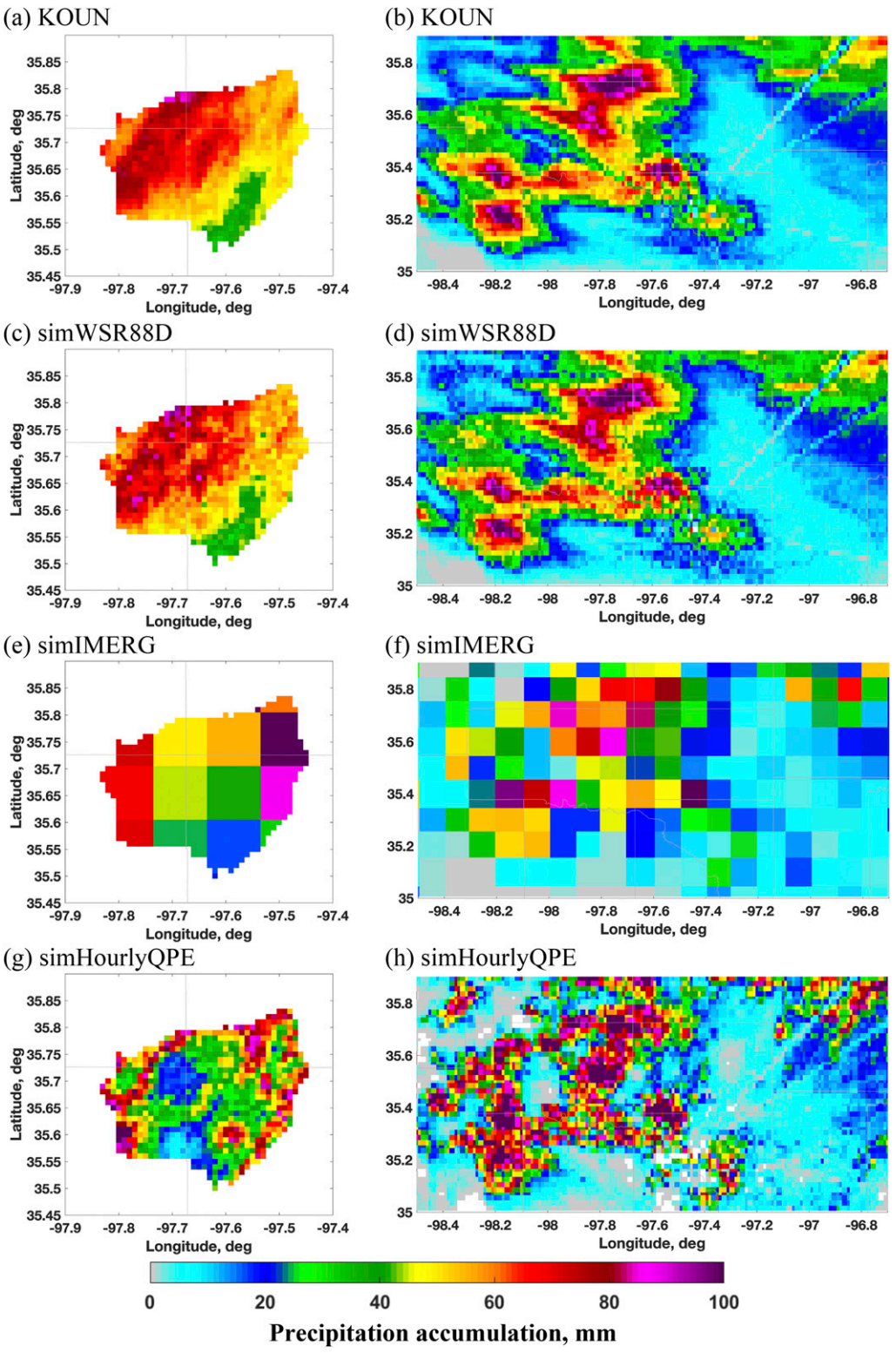


FIG. 3. Precipitation event accumulations for (left) 29 Apr 2017 in the Cottonwood Creek Basin and (right) 14 Aug 2018 in Oklahoma City area.

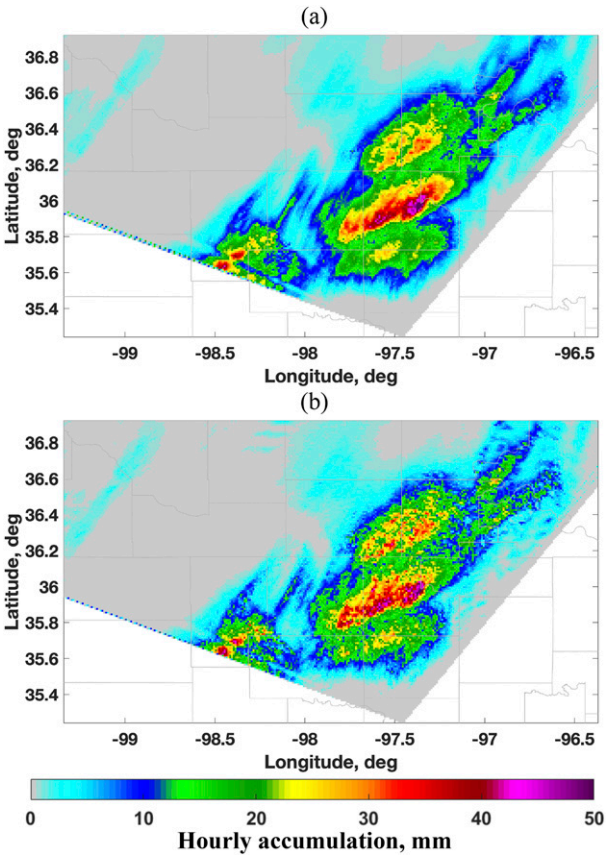


FIG. 4. Hourly accumulation from 0700 to 0800 UTC 29 Apr 2017 derived from (a) KOUN data with 1-min temporal resolution and (b) simWSR88D data with 5-min temporal resolution.

- The discharge and unit discharge forced by KOUN 1-km/1-min precipitation product are simulated and taken as truth.
- KOUN rainfall data are resampled into different spatial and temporal resolutions.
- The EF5 is rerun with simulated precipitation fields of coarser resolutions.
- The newly simulated discharges are then compared with those simulated using the original KOUN observations to assess the propagation of the precipitation sampling errors.

## 3. High variability of precipitation from a case-study perspective

In this section, we present two central Oklahoma flash flood events where the hydrologic modeling covered by the high spatial and temporal sampling of precipitation. The first event occurred on 29 April 2017. During this event, widespread rain and high winds impacted much of Oklahoma. Interstate 235 from North Oklahoma City to Edmond was closed for several hours because of flooding (source: https://okcfox.com/news/local/heavy-storms-bring-flooding-road-closures-to-oklahoma). Widespread flooding of roads with depths up to one foot in Edmond was reported to NWSChat, an instant messaging program utilized by NWS operational personnel to share significant weather information (https://nwschat.weather.gov/). A press release from the Oklahoma Governor's office declared a state of emergency in response to a night of heavy storms. Central and eastern Oklahoma remained under a flash flood watch as storms continued tracking through the state the next day (https://oklahoma.gov/oem/emergencies-and-disasters/2017/20170429-severe-weather-and-flooding-event.html). As noted in section 2, rapid-update KOUN data during this event were collected over a 90° sector that was focused toward the north from 0353 to 1308 UTC (Fig. 1a). Due to the limited rainfall sampling area resulting from the 90° sector scan used for the data collection, the study area for this case is only one single basin, the Cottonwood Creek basin near Seward, Oklahoma (USGS hydrologic unit 07159750), which has a drainage area of 828 $km^2$. Storm total rainfall accumulations from KOUN in this basin exceeded 100 mm with the greatest accumulation extending in a southwest–northeast-oriented band over the northwest bound of the Cottonwood Creek basin (Fig. 2a).

The second event started the evening of 14 August 2018. During this event, severe flooding inundated the Oklahoma City area, resulting in the Oklahoma City Fire Department responding to more than 30 calls for assisting vehicles stranded in high water at different locations around the city (source: https://www.news9.com/story/5e35da462f69d76f6201b399/flash-flood-watch-for-most-of-eastern-oklahoma). As noted in section 2, low-elevation KOUN data were collected over a full 360° azimuth with a volume update time of ~1 min from 2037 UTC 14 August to 0900 UTC 15 August 2018 during this event. Since KOUN provided a large area of rainfall observations, the study area of this case includes multiple basins centered on the area of highest flash flooding impact (98.5°–96.9°W, 35.0°–35.9°N). The maximum 12-h storm rainfall accumulations from KOUN approached 100 mm with the greatest accumulations over southern Oklahoma City and northern Norman (Fig. 2b).

Figures 3a–h show maps of total precipitation accumulation from the four products for the 29 April 2017 and 14 August 2018 events. KOUN data with resolution of 1 km/1 min (Figs. 3a,b) are used as a reference for total precipitation comparison. Figures 3c and 3d show that the KOUN and simWSR88D (1 km/5 min) products are fairly consistent in capturing the precipitation pattern in the research area, although simWSR88D shows an overestimation compared to KOUN at ~36.65°N, 97.65°W (Fig. 3c) on 29 April 2017. However, large discrepancies exist compared to KOUN for simIMERG (10 km/30 min) and simHourly (1 km/60 min). For 29 April 2017, simIMERG fails to show the precipitation pattern or the gradient of precipitation decreasing along a northwest–southeast direction, while simHourly presents extremely low precipitation to the east of the heavy rainband (35.7°N, 97.7°W) and a false area of high rainfall north of Oklahoma City (35.6°N, 97.6°W). For 14 August 2018, simIMERG and simHourlyQPE capture the general areal extent of the precipitation but fail to indicate where the heaviest rain actually fell. Both cases demonstrate that observations with coarse spatial and temporal sampling can cause large errors in quantifying precipitation amount.

Coarse sampling also causes errors in quantifying precipitation intensity and distribution. Figure 4 displays maps of hourly rainfall accumulation from 0700 to 0800 UTC 29 April

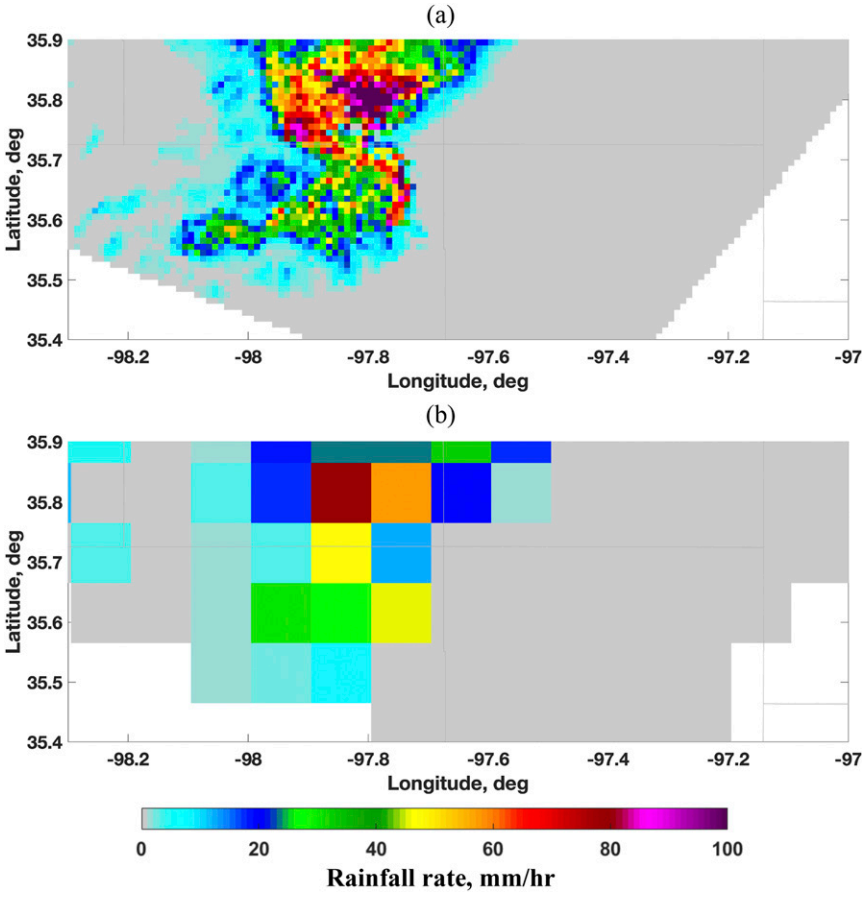


FIG. 5. Rainfall rate at 0700 UTC 29 Apr 2017 from (a) KOUN of 1-km spatial resolution and (b) simIMERG of 10-km spatial resolution.

2017 derived from KOUN data with 1-min temporal resolution and from simWSR88D data with 5-min temporal resolution. The KOUN hourly accumulation shows smooth rain fields, while the simWSR88D hourly accumulation has discontinuities. Figure 5 shows the rainfall rate observed at 0700 UTC 29 April 2017 by KOUN at 1-km spatial resolution and simIMERG at 10-km spatial resolution. The fine-scale rainfall patterns are lost when spatial resolution is coarser. Over- and underestimation errors can be identified by the difference between KOUN precipitation rate and simIMERG rainfall rates (Fig. 5). These discrepancies are due to the high spatial and temporal variability of natural precipitation and are important to consider because these errors will negatively affect hydrologic simulations and applications.

## 4. Flash flood simulations using different precipitation products

Figure 6 shows the time series of rainfall rates and simulated discharges at the Cottonwood Creek stream gauge near Seward, Oklahoma (USGS hydrologic unit 07159750) on 29 April 2017. As can be seen in Fig. 6b, the peak rain rate decreases as the temporal resolution gets coarser. It is also evident that the precipitation bias results from poor spatial and temporal sampling propagates in the streamflow simulations. Figure 6c shows that the discharge generated by rapid-update KOUN data better matches stream gauge observations than those generated by the precipitation products with coarser resolution. Note that all simulations underestimate discharge compared to the stream gauge observations. The negative bias may come from radar measurement error, retrieval algorithm uncertainty, hydrologic model uncertainty, and precipitation sampling error. In this paper, we only consider the effects of precipitation sampling error on the flash flood forecasts. Therefore, we took simulated discharge forced by KOUN as truth to assess other simulations rather than discussing the underestimation of all the simulations compared to the stream gauge observations. Compared to peak discharge from KOUN at the stream gauge location, the peak discharge from simWSR88D, simIMERG, and simHourly is reduced by ~10%, 33%, and 43%, respectively.

Figure 7 presents the EF5 peak unit discharge product forced by KOUN observations for the two cases. On 29 April 2017, peak unit discharges exceed $3\,m^3\,s^{-1}\,km^{-2}$ in the southeastern part of the basin (Fig. 7a), which is consistent with NWSChat reports. It is interesting to point out that the heaviest precipitation occurred in the northwestern part of the

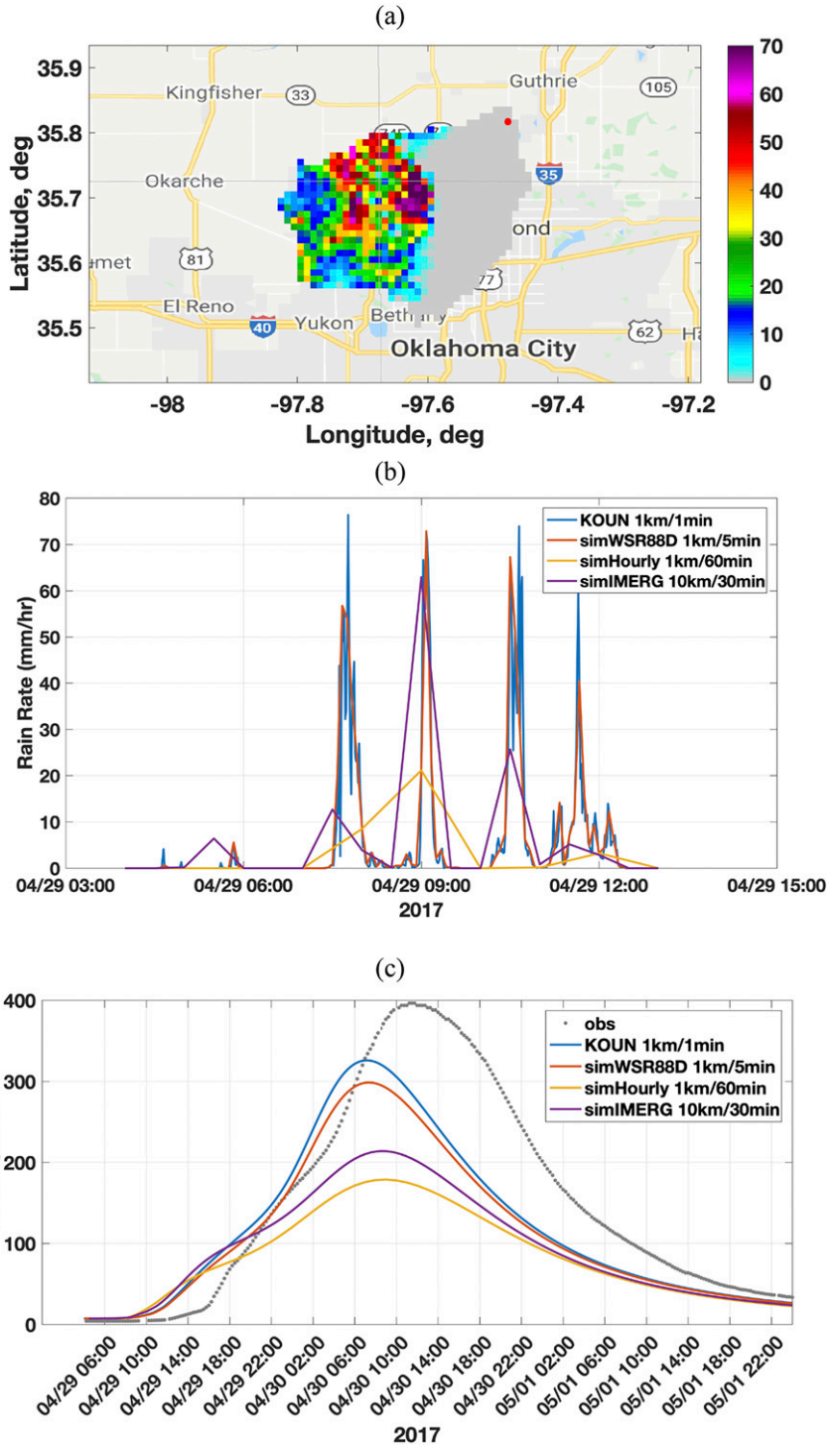


FIG. 6. (a) Example of instantaneous rainfall rate measured by KOUN at 0718 UTC 29 Apr 2017. (b) The time series data of different precipitation data at different temporal-spatial resolutions. (c) The time series data of simulated streamflow simulated from different precipitation data. In (c), the dotted gray line is observation from a USGS stream gauge (Cottonwood Creek near Seward, USGS hydrologic unit 07159750). The location of the time series data is from the stream gauge noted by the red dot in (a).

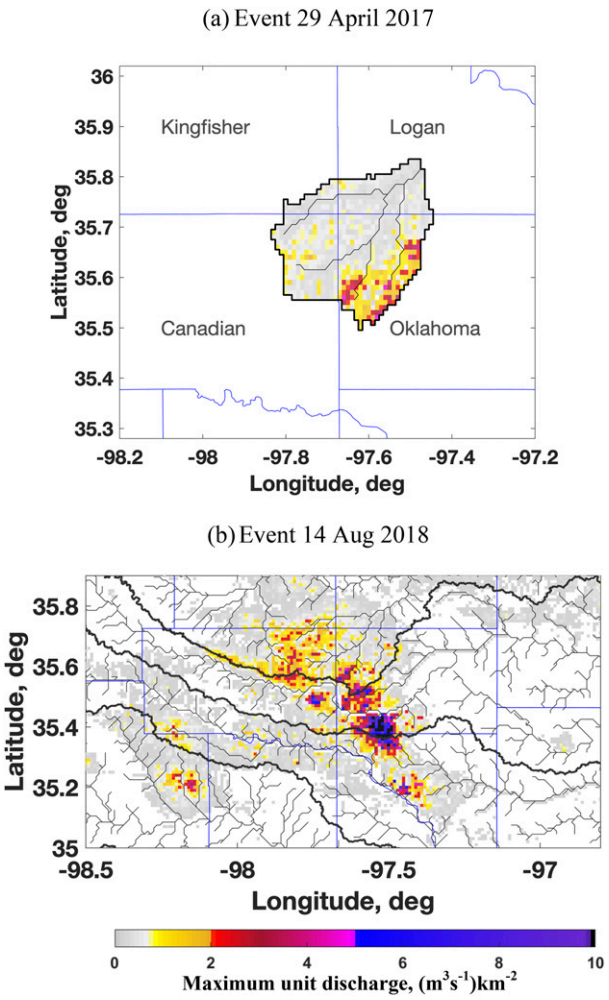


FIG. 7. Maximum unit discharge simulation using KOUN 1-min/1-km observations (a) from 0300 UTC 29 Apr 2017 to 0000 UTC 2 May 2017 and (b) from 2100 UTC 14 Aug 2018 to 0000 UTC 17 Aug 2018. The thick black lines indicate the boundaries of the basins, the thin black lines indicate the main streams, and the blue lines are the county boundaries.

basin (Fig. 3a), not in the southeastern part where the most severe flooding impacts were reported. Due to the extent in impervious surfaces in the Oklahoma City metropolitan area, the EF5 model has very low or no infiltration in some areas, resulting in high values of runoff. The location mismatch of heaviest precipitation and flash flood occurrence indicate that the precipitation errors do not propagate linearly in the flash flood simulation. Basin physiographic and morphological characteristics, such as basin slope, drainage ratio, basin magnitude, infiltration rates, ruggedness number, etc., will influence the effects of precipitation sampling errors on flash flood forecasts. The peak unit discharge for 14 August 2018 is displayed in Fig. 7b. The peak unit discharge exceeds $6\,m^3\,s^{-1}\,km^{-2}$ in southern Oklahoma City, corresponding closely with media reports.

The magnitude of peak unit discharges simulated from coarse-resolution precipitation products are assessed by comparing them to the KOUN simulations (Fig. 8). The simWSR88D simulations (Fig. 8a) show a consistent negative bias over the study area for both events, while simIMERG (Fig. 8b) and simHourly (Fig. 8c) simulations have both positive and negative biases when compared to KOUN simulations. In particular, it is easy to notice that the spatial patterns of the bias for simIMERG-based simulations (Fig. 8b) depict the 10-km grid pixel. This is due to the higher spatial resolution of the hydrologic model's computational grid. The right column of Figs. 8b and 8c shows that the area of positive bias is adjacent to the area of negative bias, which indicates simIMERG and simHourly sampling frequency has difficulty capturing the movement of precipitation in fast-moving storms or isolated convective system.

To estimate the negative impact on forecasting flash flood occurrence due to the degradation of resolution, simple metrics derived from contingency table statistics (i.e., POD, FAR, and CSI) are used. We assumed the unit discharge of $1.5\,m^3\,s^{-1}\,km^{-2}$ was the flash flood threshold and grid points with unit discharge of KOUN simulations greater than 1.5 are marked as flash flood grid points. Then we counted the number of the hits, misses, and false alarms of other QPE-based simulations. Table 2 shows the POD, FAR, and CSI for hydrological simulations forced by the simWSR88D, simIMERG, and simHourly precipitation products. Table 3 shows the RB, MAE, and RMSE for hydrologic simulations by the simWSR88D, simIMERG, and simHourly benchmarked by KOUN. The quantitative evaluation statistics indicates the hydrologic simulation from simWSR88D only has slight underestimation. The 29 April 2017 event is not a significant flash flood event, which means the streamflow peak barely passes the flash flood threshold in many grids. A slight underestimation of streamflow would be below the threshold and thus misses the flash flood event. Overall, simWSR88D data have the highest capacity to detect flash flood area compared to simIMERG and simHourly. On 29 April 2017, the quantitative evaluation statistics indicates the hydrologic simulation from simWSR88D only has slight underestimation; however, simWSR88D data have a low POD of 0.46, indicating that simWSR88D data missed more than 50% of the flash flooding grid points.

Nijssen and Lettenmaier (2004) studied the effect of error in accumulated precipitation at $0.5° \times 0.5°$ spatial resolution, due to periodic sampling (1, 3, and 6 h) of the precipitation rate, and found that streamflow errors were large for small drainage areas ($5 \times 10^3\,km^2$) and generally decrease for drainage areas up to $500 \times 10^3\,km^2$. In this study, we also investigated the effect of precipitation sampling errors as a function of upstream drainage area but at the flash flood scale (i.e., drainages $< 1000\,km^2$), where information with higher resolution is required. Examples of streamflow time series with different drainage areas are presented in Fig. 9, from a $1\text{-km}^2$ drainage area to a river channel of $916\,km^2$. With drainage area increasing, the hydrographs change from narrow and sharp depicting flashy response typical of basin headwaters, to wide and smooth depicting slower response typical of main river stems. In addition, the differences between KOUN simulations and simWSR88D simulations diminish as drainage area increases. The behavior of the simIMERG and simHourly

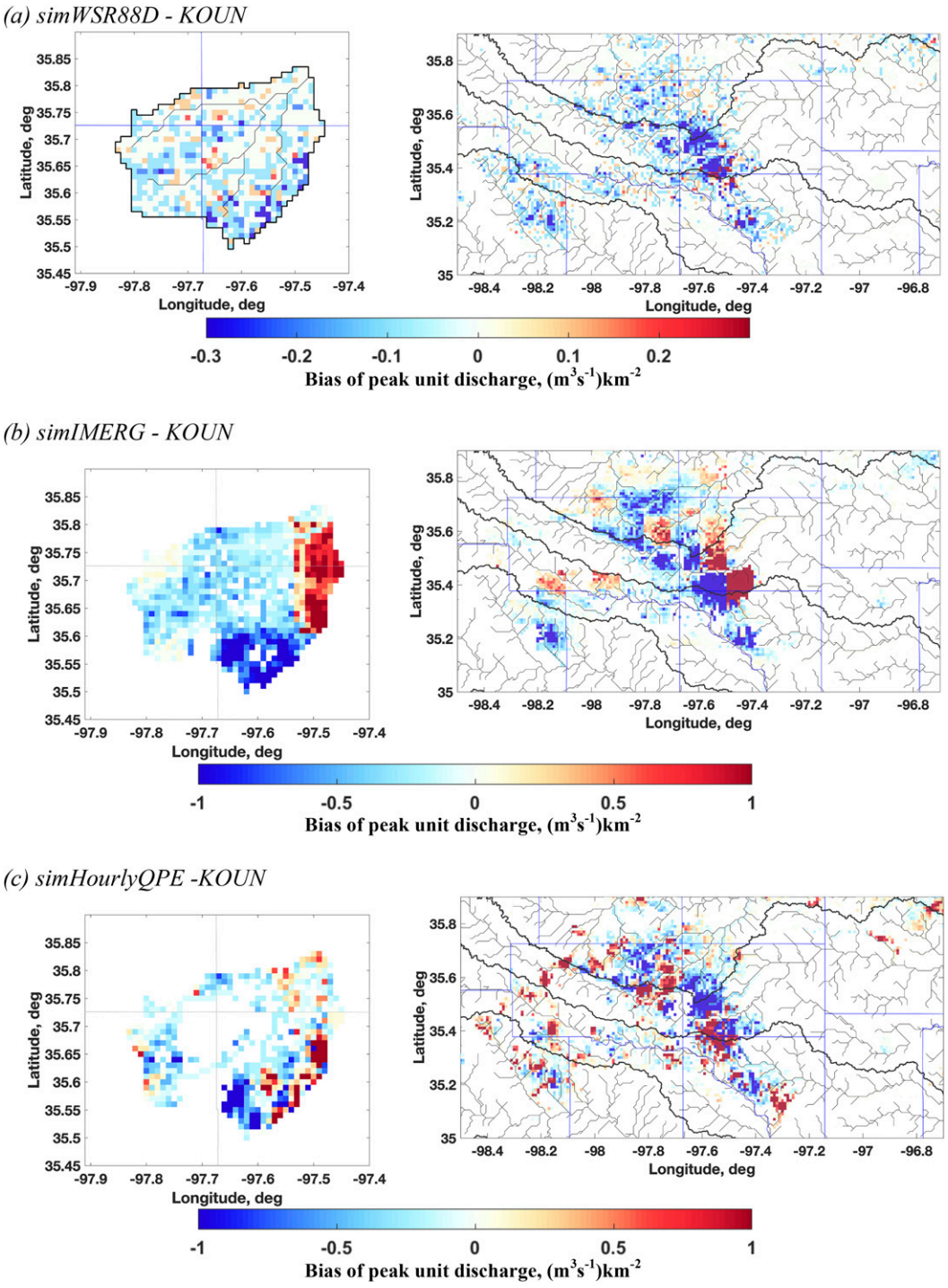


FIG. 8. Bias of peak unit discharge forced by (a) simWSR88D, (b) simIMERG, and (c) simHourly, compared to the unit peak discharge simulated by KOUN for (left) 29 Apr 2017 and (right) 14 Aug 2018. Note that to demonstrate the small bias of simWSR88D in (a), the color bar ranges from $-0.3$ to $0.3\ m^3\ s^{-1}\ km^{-2}$, while in (b) and (c) color bars range from $-1$ to $1\ m^3\ s^{-1}\ km^{-2}$.

simulation time series at a single grid is not enough to explain the effects of sampling errors in precipitation, as the 60-min snapshot temporal sampling intrinsically create dramatic random error in precipitation and the averaging of all fine 1-km resolution grids into 10-km grid also causes large over- and underestimation errors. A larger statistical sample is

TABLE 2. The contingency table statistics benchmarked by KOUN simulations. The best performance according to the statistic is denoted in boldface.

| Event date | QPE products | POD | FAR | CSI |
|---|---|---|---|---|
| 29 Apr 2017 | simWSR88D | **0.46** | **0.33** | **0.38** |
| | simIMERG | 0.08 | 0.98 | 0.01 |
| | simHourly | 0.38 | 0.98 | 0.02 |
| 14 Aug 2018 | simWSR88D | **0.83** | **0.00** | **0.83** |
| | simIMERG | 0.36 | 0.50 | 0.26 |
| | simHourly | 0.48 | 0.72 | 0.22 |

needed to analyze the drainage area impact over the whole study area.

Figure 10 shows the statistics (RB, MAE, and RMSE) of unit discharge relative to basin area using KOUN simulations as a benchmark. All statistics show a trend of improving values with increasing basin area, consistent with the findings in Nijssen and Lettenmaier (2004). The simWSR88D data show the best statistics among the three precipitation products as we expected. As shown in Fig. 10, the simIMERG simulations have lower MAE and RMSE than the simHourly simulations indicating the streamflow simulation driven by QPE at 10-km/30-min resolution is better than that driven by QPE at 1-km/1-h resolution. The degraded temporal resolution (1 h vs 30 min) has larger negative impact on flash flooding discharge simulations than the spatial resolution (10 vs 1 km). This result indicates the importance of temporal resolution of precipitation input on flash flooding warning.

## 5. Probabilistic study of the different precipitation products

Since both radars and satellites essentially take instantaneous ''snapshot'' measurements, the KOUN 1-km/1-min rainfall field was selected every 5th, 30th, and 60th time step to mimic the WSR-88D, IMERG, and hourly QPE products, respectively. However, the hydrologic uncertainties quantified by different temporal resolutions derived from a deterministic method could be incomplete. For example, if the fifth time step of rainfall rate is the lowest value among the five 1-min observations in a 5-min period, the hydrologic simulation will probably yield a very low discharge. If the fifth time step of rainfall rate is the highest in the 5-min period, the hydrologic simulation will be very close to the 1-min benchmark. To evaluate the impact of the different precipitation products, a probabilistic approach is adopted to simulate the distributions of precipitation rates at different resolutions. A probabilistic description of the QPE products is most appropriate to acknowledge the possible range of outputs from the 5-min, 30-min, and 60-min simulations that might result from sampling the 1-min KOUN data.

To describe this approach, we use the derivation of probabilistic 5-min QPE products. First, we generate 50 random numbers from Student's $t$ distribution since the sample size is small. Then we calculate the mean and standard deviation of the sample mean of the five 1-min rainfall rate within each

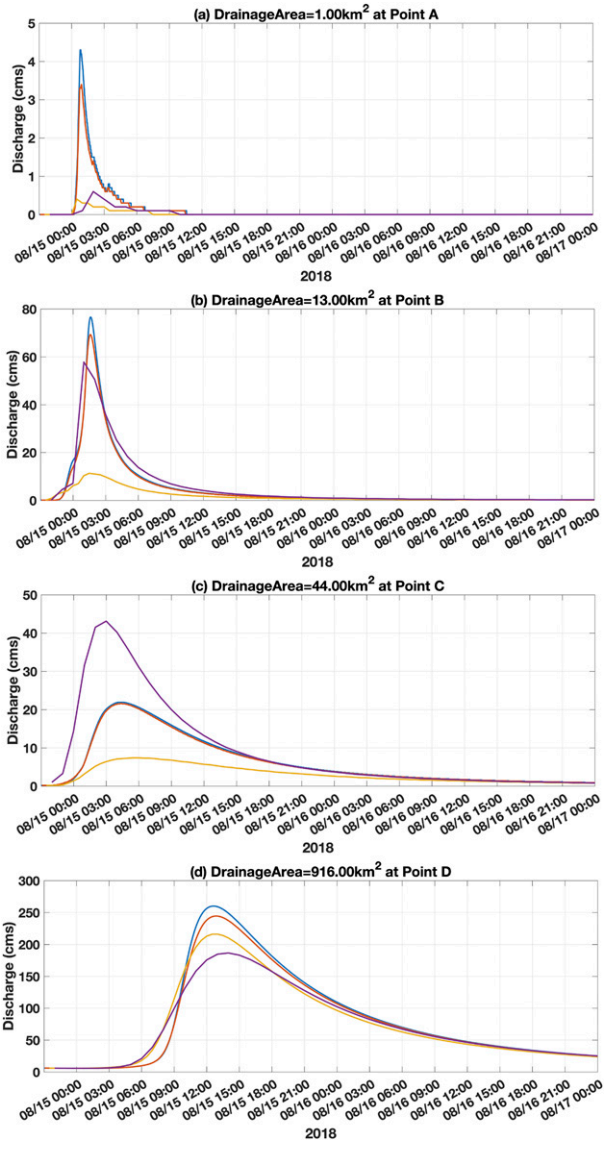


FIG. 9. Time series of simulated discharge from different locations of different drainage areas: (a) from drainage area of 1 km$^2$ (location A denoted as a black dot in Fig. 7b), (b) from drainage area of 13 km$^2$ (point B in Fig. 7b), (c) from drainage area of 44 km$^2$ (point C in Fig. 7b), and (d) from drainage area of 916 km$^2$ (point D in Fig. 7b).

TABLE 3. Statistical results of the maximum unit discharge benchmarked by KOUN simulations. The best performance according to the statistic is denoted in boldface.

| Event date | QPE products | RB (%) | MAE | RMSE |
|---|---|---|---|---|
| 29 Apr 2017 | simWSR88D | **−7.45** | **0.04** | **0.10** |
| | simIMERG | 4.11 | 0.26 | 0.55 |
| | simHourly | 98.11 | 0.58 | 1.63 |
| 14 Aug 2018 | simWSR88D | **−7.96** | **0.04** | **0.11** |
| | simIMERG | −17.01 | 0.35 | 0.97 |
| | simHourly | 32.50 | 0.47 | 1.03 |

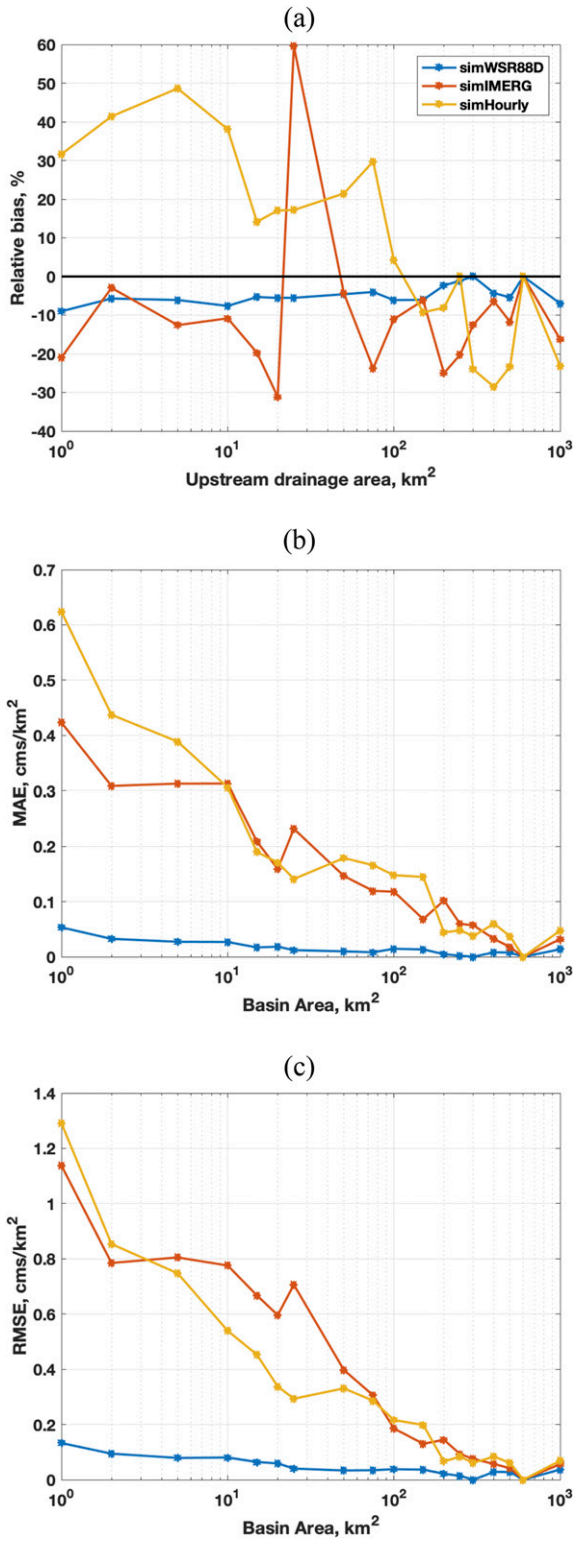


FIG. 10. Statistical results of simulated unit discharge as a function of drainage area with KOUN simulations as reference.

5-min interval. Next, we use the mean and standard deviation of the sample mean to scale the 50 random numbers and make them statistically match the five 1-min rainfall rate observations. Finally, 50 sets of 5-min QPE products are generated from the 1-min baseline product and are used to drive the EF5 hydrologic model. The same approach is also applied to derive 50 sets of 30-min QPE products and 50 sets of hourly QPE products.

The example of discharge time series from probabilistic precipitation products is shown in Fig. 11. The medians of 50 members of hydrologic simulations from each QPE with coarser resolution are also presented in Fig. 11. There are two members of discharge simulation from simWSR88 5-min product having a higher peak discharge than the 1-min baseline simulation. However, the ensemble median value of the 50 discharge simulations of the 5-min product has a lower peak discharge than the 1-min simulation. The median of simulations from hourly QPE products has the lowest peak discharge of the four resolution QPE products. The results of probabilistic QPE simulations are consistent with the deterministic simulation results in previous sections.

Figure 12 shows the distribution of statistics (RB, MAE, and RMSE) of unit discharge relative to basin area using KOUN simulations as a benchmark. Similar to the results shown in Fig. 10, the ensemble median of all statistics shows a trend of improving values with increasing basin area. The simWSR88D output shows the best statistics (lowest RB, MAE, and RMSE) among the three precipitation products and smallest standard deviation from the median value for MAE (Fig. 12b) and RMSE (Fig. 12c). The simIMERG has the largest standard deviation when basin area is smaller than 100 km$^2$. This result is consistent with simIMERG's spatiotemporal resolution of 10 km. The distribution of the simIMERG simulations has lower MAE and RMSE than the simHourly simulations in small basin areas indicating the stream flow simulation driven by QPE at 10-km/30-min resolution is better than that driven by 1-km/1-h products when the basin area is small. The degraded temporal resolution (1 h vs 30 min) has a larger negative impact on flash flooding simulations than the degraded spatial resolution (10 vs 1 km) for small basins. However, when basin area is greater than 20 km$^2$, the MAE and RMSE are similar to 10-km/30-min and 1-km/1-h products.

## 6. Summary and conclusions

This study demonstrates the high variability of precipitation captured by rapid-update KOUN radar observations and investigates its hydrologic impacts on flash flood simulations. The effect of precipitation sampling errors on flash flood forecasting was investigated using rapid-update KOUN precipitation observations at 1 km × 1 km resolution updating every ~1 min to force the EF5 hydrological model. The simulated discharge from KOUN was then used as truth to assess simulations from three other precipitation products that had degraded spatial and/or temporal resolutions. The main findings are summarized as follows:

1) Observations with coarse spatial and temporal sampling can cause large errors when quantifying precipitation amount,

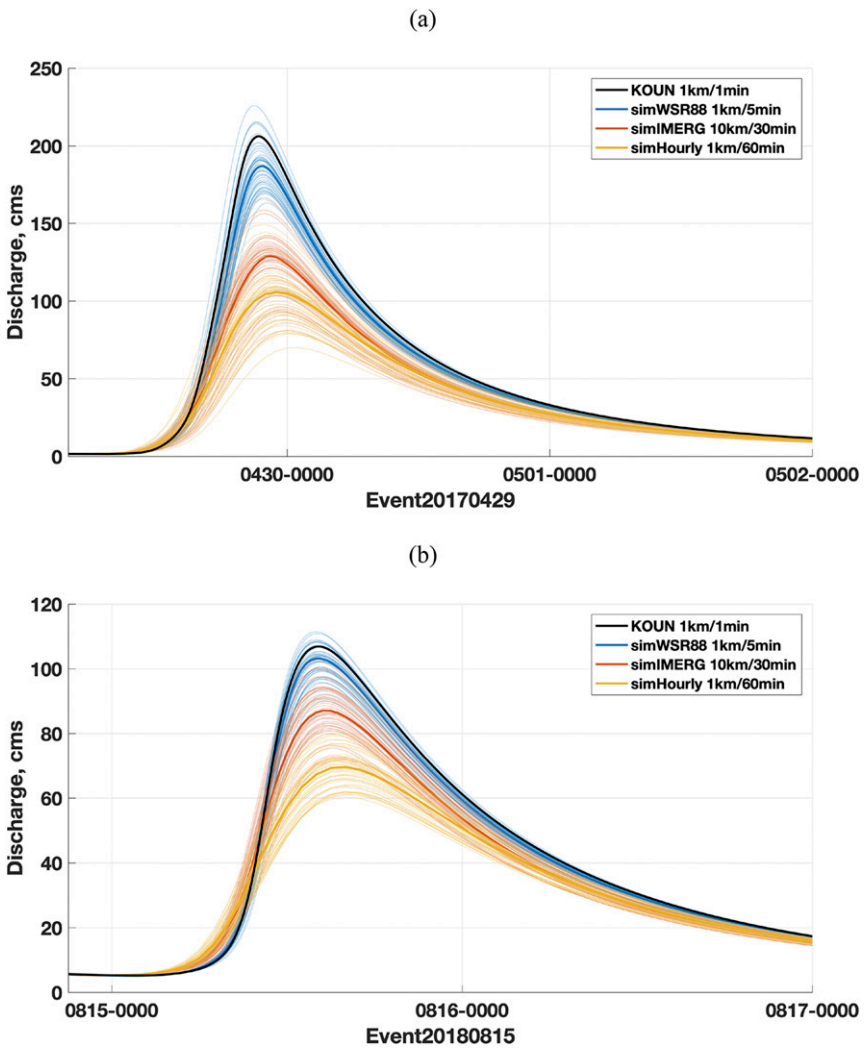


FIG. 11. Time series of simulated discharge from different probabilistic precipitation products from (a) 29 Apr 2017 and (b) 15 Aug 2018. The light lines indicate the simulations from 50 members, and the thick lines indicate the median value of 50 hydrologic simulations.

intensity, and distribution. The simWSR88D (5 km/1 min) products are fairly consistent with KOUN (1 km/1 min) products in precipitation event accumulations, while simIMERG (10 km/30 min) and simHourly (1 km/60 min) showed large discrepancies when compared to KOUN storm accumulation. The KOUN hourly accumulation showed smooth rain fields, while the simWSR88D hourly accumulation has discontinuities.

2) Time series of precipitation products showed that QPE peak value decreased as the temporal resolution got coarser. Discharge simulated from KOUN better matched stream gauge observations than those generated by the coarser resolution precipitation products. Compared to KOUN simulations for 29 April 2017, the peak discharge from the simWSR88D, simIMERG, and simHourlyQPE simulations was smaller by ~10%, 33%, and 43%, respectively.
3) The simWSR88D data had the highest detectability in terms of POD when using a flash flood threshold of $1.5\,m^3\,s^{-1}\,km^{-2}$, but the CSI of simWSR88D simulations was as low as 0.46 for the 29 April 2017 case.
4) The effect of precipitation sampling error on flash flood forecasting was dependent on upstream drainage area. Streamflow errors were large in headwater basin areas and decrease quickly as drainage area increases. Metropolitan areas located in headwater areas would have the greatest need for rapid-update KOUN precipitation data.
5) The probabilistic approach shows that the degraded temporal resolution has a larger negative impact on flash flooding simulations than the degraded spatial resolution for small basins.

The mismatch of heaviest precipitation area and flash flood impacted area indicated that the effect of precipitation

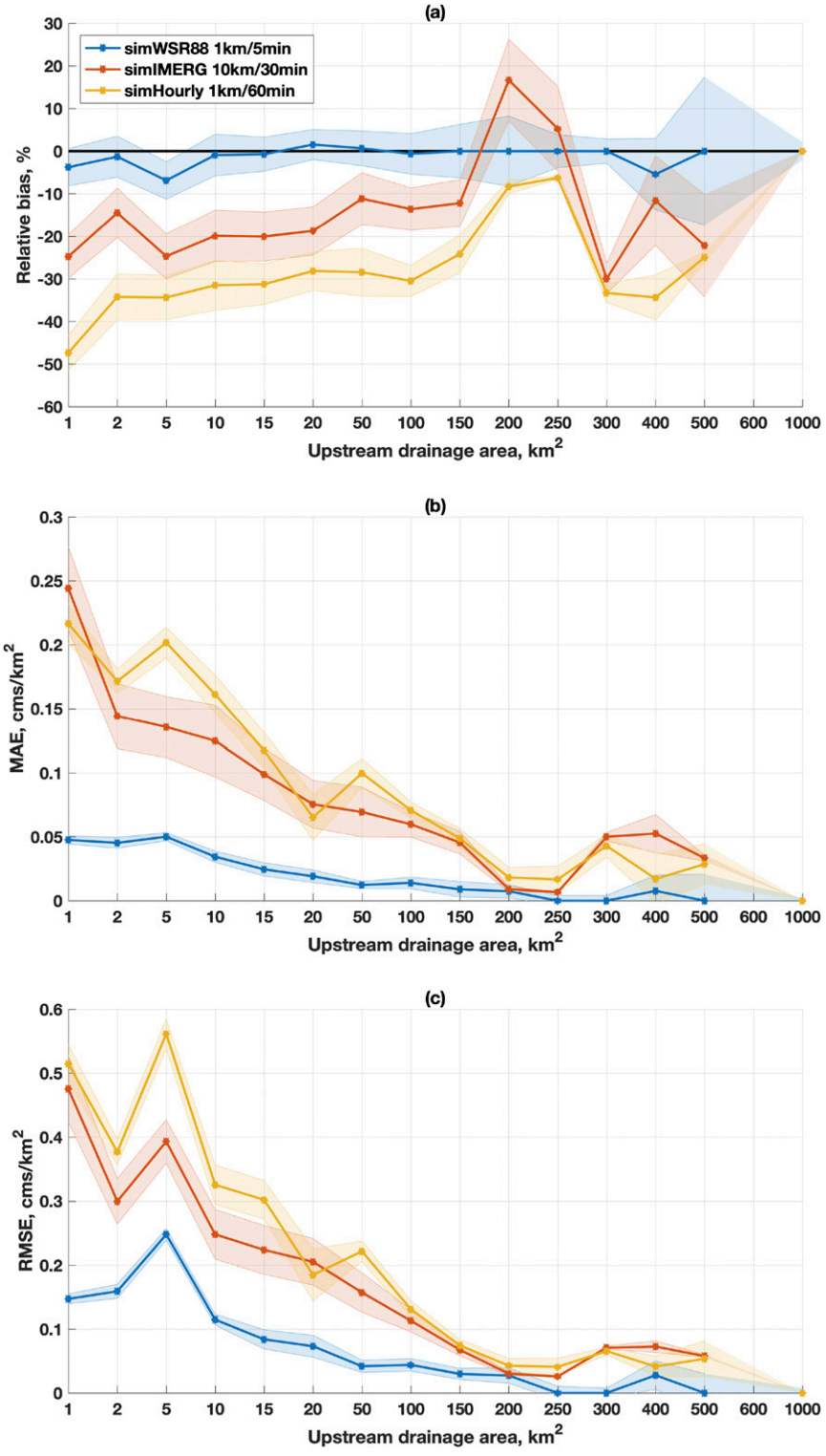


FIG. 12. Distribution of statistics of simulated unit discharge as a function of drainage area with KOUN simulations as reference. The thick lines represent the ensemble median of statistics and the shaded area represent one standard deviation from the ensemble median.

sampling errors on hydrologic simulation may be influenced by basin physiographic and morphological characteristics. When this research is extended to the whole country, basin morphology needs to be considered to decide the regions that need rapid-update radar precipitation observations the most. Such analyses can provide hydrologic insights for future upgrades to the current operational WSR-88D network. A future PAR network with rapid-update scanning ability could benefit the hydrologic and meteorological communities by decreasing precipitation errors resulting from degraded spatial and temporal sampling, and therefore improve flash flood monitoring.

*Acknowledgments.* The authors thank Drs. J. J. Gourley and Zac Flamig for helpful discussions during the preparation of this manuscript; John Krause for processing polarimetric radar QPE; and Dr. Pierre Kirstetter for help on probabilistic approach. Funding was provided by the Spectrum Efficient National Surveillance Radar (SENSR) program and the NOAA/Office of Oceanic and Atmospheric Research under NOAA-University of Oklahoma Cooperative Agreement NA16OAR4320115, U.S. Department of Commerce.

## REFERENCES

Anagnostou, M. N., and Coauthors, 2018: Advancing precipitation estimation and streamflow simulations in complex terrain with X-band dual-polarization radar observations. *Remote Sens.*, **10**, 1258, https://doi.org/10.3390/rs10081258.

Ashley, S. T., and W. S. Ashley, 2008: Flood fatalities in the United States. *J. Appl. Meteor. Climatol.*, **47**, 805–818, https://doi.org/10.1175/2007JAMC1611.1.

Bartsotas, N. S., E. N. Anagnostou, E. I. Nikolopoulos, and G. Kallos, 2018: Analyzing satellite QPE underestimation over mountainous terrain: A NWP-based microphysical investigation. *Geophysical Research Abstracts*, Vol. 20, Abstract EGU2018-15952, https://meetingorganizer.copernicus.org/EGU2018/EGU2018-15952.pdf.

Behrangi, A., and Y. Wen, 2017: On the spatial and temporal sampling errors of remotely sensed precipitation products. *Remote Sens.*, **9**, 1127, https://doi.org/10.3390/rs9111127.

Berne, A., G. Delrieu, J.-D. Creutin, and C. Obled, 2004: Temporal and spatial resolution of rainfall measurements required for urban hydrology. *J. Hydrol.*, **299**, 166–179, https://doi.org/10.1016/S0022-1694(04)00363-4.

Brown, R. A., V. T. Wood, and D. Sirmans, 2002: Improved tornado detection using simulated and actual WSR-88D data with enhanced resolution. *J. Atmos. Oceanic Technol.*, **19**, 1759–1771, https://doi.org/10.1175/1520-0426(2002)019<1759:ITDUSA>2.0.CO;2.

Burgess, D., V. Melnikov, D. Priegnitz, R. A. Brown, P. L. Heinselman, E. R. Mansell, and V. T. Wood, 2014: Tornadic supercells in central Oklahoma on May 19, 20, and 31 of 2013: NSSL radar data. *Proc. Special Symp. on Severe Local Storms: The Current State of the Science and Understanding Impacts*, Atlanta, GA, Amer. Meteor. Soc., 825, https://ams.confex.com/ams/94Annual/webprogram/Paper233974.html.

Chrisman, J. N., 2014: Multiple Elevation Scan Option for SAILS (MESO-SAILS)—The next step in dynamic scanning for the WSR-88D. WSR-88D Radar Operations Center, 27 pp., https://www.roc.noaa.gov/WSR88D/PublicDocs/NewTechnology/MESO-SAILS_Description_Briefing_Jan_2014.pdf.

Clark, R. A. III, and Coauthors, 2017: Hydrological modeling and capacity building in the Republic of Namibia. *Bull. Amer. Meteor. Soc.*, **98**, 1697–1715, https://doi.org/10.1175/BAMS-D-15-00130.1.

Federal Coordinator for Meteorological Services and Supporting Research, 2013: Part A: System concepts, responsibilities, and procedures. Doppler Radar Meteorological Observations, Federal Meteorological Handbook 11, U.S. Department of Commerce Doc. FCM-H11A-2013, 49 pp., https://www.ofcm.gov/publications/fmh/allfmh2.htm.

Flamig, Z. L., H. Vergara, and J. J. Gourley, 2020: The Ensemble Framework for Flash Flood Forecasting (EF5) v1.2: Description and case study. *Geosci. Model Dev.*, **13**, 4943–4958, https://doi.org/10.5194/gmd-13-4943-2020.

Giangrande, S. E., and A. V. Ryzhkov, 2008: Estimation of rainfall based on the results of polarimetric echo classification. *J. Appl. Meteor. Climatol.*, **47**, 2445–2462, https://doi.org/10.1175/2008JAMC1753.1.

Gourley, J. J., and Coauthors, 2011: Hydrologic evaluation of rainfall estimates from radar, satellite, gauge, and combinations on Ft. Cobb Basin, Oklahoma. *J. Hydrometeor.*, **12**, 973–988, https://doi.org/10.1175/2011JHM1287.1.

——, and Coauthors, 2017: The FLASH Project: Improving the tools for flash flood monitoring and prediction across the United States. *Bull. Amer. Meteor. Soc.*, **98**, 361–372, https://doi.org/10.1175/BAMS-D-15-00247.1.

Heinselman, P. L., and S. M. Torres, 2011: High-temporal-resolution capabilities of the National Weather Radar Testbed phased array radar. *J. Appl. Meteor. Climatol.*, **50**, 579–593, https://doi.org/10.1175/2010JAMC2588.1.

Hossain, F., and E. N. Anagnostou, 2004: Assessment of current passive-microwave- and infrared-based satellite rainfall remote sensing for flood prediction. *J. Geophys. Res.*, **109**, D07102, https://doi.org/10.1029/2003JD003986.

Huffman, G. J., and Coauthors, 2020: Integrated Multi-satellitE Retrievals for the Global Precipitation Measurement (GPM) mission (IMERG). *Satellite Precipitation Measurement*, V. Levizzani et al., Eds., Advances in Global Change Research Series, Vol. 67, Springer Nature, 343–353.

Kidd, C., A. Becker, G. J. Huffman, C. L. Muller, P. Joe, G. Skofronick-Jackson, and D. B. Kirschbaum, 2017: So, how much of the Earth's surface is covered by rain gauges?. *Bull. Amer. Meteor. Soc.*, **98**, 69–78, https://doi.org/10.1175/BAMS-D-14-00283.1.

Maggioni, V., H. J. Vergara, E. N. Anagnostou, J. J. Gourley, Y. Hong, and D. Stampoulis, 2013: Investigating the applicability of error correction ensembles of satellite rainfall products in river flow simulations. *J. Hydrol.*, **14**, 1194–1211, https://doi.org/10.1175/JHM-D-12-074.1.

Martinaitis, S. M., and Coauthors, 2017: The HMT multi-radar multi-sensor hydro experiment. *Bull. Amer. Meteor. Soc.*, **98**, 347–359, https://doi.org/10.1175/BAMS-D-15-00283.1.

Nai, F., S. M. Torres, and R. D. Palmer, 2016: Adaptive beamspace processing for phased-array weather radars. *IEEE Trans. Geosci. Remote Sens.*, **54**, 5688–5698, https://doi.org/10.1109/TGRS.2016.2570138.

National Research Council, 2002: *Weather Radar Technology Beyond NEXRAD*. National Academies Press, 97 pp., https://doi.org/10.17226/10394.

Nijssen, B., and D. P. Lettenmaier, 2004: Effect of precipitation sampling error on simulated hydrological fluxes and states: Anticipating the global precipitation measurement satellites. *J. Geophys. Res.*, **109**, D02103, https://doi.org/10.1029/2003JD003497.

Park, H., A. V. Ryzhkov, D. S. Zrnic, and K. E. Kim, 2009: The hydrometeor classification algorithm for the polarimetric WSR-88D: Description and application to an MCS. *Wea. Forecasting*, **24**, 730–748, https://doi.org/10.1175/2008WAF2222205.1.

Rafieeinasab, A., and Coauthors, 2015: Toward high-resolution flash flood prediction in large urban areas—Analysis of sensitivity to spatiotemporal resolution of rainfall input and hydrologic modeling. *J. Hydrol.*, **531**, 370–388, https://doi.org/10.1016/j.jhydrol.2015.08.045.

Ryzhkov, A. V., and D. S. Zrnic, 2019: *Radar Polarimetry for Weather Observations*. Springer, 475 pp.

——, S. E. Giangrande, and T. J. Schuur, 2005a: Rainfall estimation with a polarimetric prototype of WSR-88D. *J. Appl. Meteor.*, **44**, 502–515, https://doi.org/10.1175/JAM2213.1.

——, T. J. Schuur, D. W. Burgess, P. L. Heinselman, S. E. Giangrande, and D. S. Zrnić, 2005b: The Joint Polarization Experiment: Polarimetric rainfall measurements and hydrometeor classification. *Bull. Amer. Meteor. Soc.*, **86**, 809–824, https://doi.org/10.1175/BAMS-86-6-809.

Stoica, P., and R. Moses, 2005: *Spectral Analysis of Signals*. Pearson, 447 pp.

Tanamachi, R. L., and P. L. Heinselman, 2016: Rapid-scan, polarimetric observations of central Oklahoma severe storms on 31 May 2013. *Wea. Forecasting*, **31**, 19–42, https://doi.org/10.1175/WAF-D-15-0111.1.

Van der Veer Martens, B., B. G. Illston, and C. A. Fiebrich, 2017: The Oklahoma Mesonet: A pilot study of environmental sensor data citations. *Data Sci. J.*, **16**, 47, https://doi.org/10.5334/dsj-2017-047.

Vergara, H., Y. Hong, J. J. Gourley, E. N. Anagnostou, V. Maggioni, D. Stampoulis, and P. E. Kirstetter, 2014: Effects of resolution of satellite-based rainfall estimates on hydrologic modeling skill at different scales. *J. Hydrometeor.*, **15**, 593–613, https://doi.org/10.1175/JHM-D-12-0113.1.

——, P.-E. Kirstetter, J. Gourley, Z. Flamig, Y. Hong, A. Arthur, and R. Kolar, 2016: Estimating a-priori kinematic wave model parameters based on regionalization for flash flood forecasting in the conterminous United States. *J. Hydrol.*, **541**, 421–433, https://doi.org/10.1016/j.jhydrol.2016.06.011.

Weber, M. E., J. Y. Cho, J. S. Herd, J. M. Flavin, W. E. Benner, and G. S. Torok, 2007: The next-generation multimission U.S. surveillance radar network. *Bull. Amer. Meteor. Soc.*, **88**, 1739–1752, https://doi.org/10.1175/BAMS-88-11-1739.

Wen, Y., Q. Cao, P.-E. Kirstetter, Y. Hong, J. J. Gourley, J. Zhang, G. Zhang, and B. Yong, 2013: Incorporating NASA spaceborne radar data into NOAA National Mosaic QPE system for improved precipitation measurement: A physically based VPR identification and enhancement method. *J. Hydrometeor.*, **14**, 1293–1307, https://doi.org/10.1175/JHM-D-12-0106.1.

——, A. Behrangi, H. Chen, and B. Lambrigtsen, 2018: How well were the early 2017 California Atmospheric River precipitation events captured by satellite products and ground-based radars? *Quart. J. Roy. Meteor. Soc.*, **144**, 344–359, https://doi.org/10.1002/qj.3253.

Wood, V. T., and R. A. Brown, 1997: Effects of radar sampling on single-Doppler velocity signatures of mesocyclones and tornadoes. *Wea. Forecasting*, **12**, 928–938, https://doi.org/10.1175/1520-0434(1997)012<0928:EORSOS>2.0.CO;2.

Zhang, J., and Coauthors, 2016: Multi-Radar Multi-Sensor (MRMS) quantitative precipitation estimation: Initial operating capabilities. *Bull. Amer. Meteor. Soc.*, **97**, 621–638, https://doi.org/10.1175/BAMS-D-14-00174.1.

Zhang, X., E. N. Anagnostou, and H. Vergara, 2016: Hydrologic evaluation of NWP-adjusted CMORPH estimates of hurricane-induced precipitation in the southern Appalachians. *J. Hydrol.*, **17**, 1087–1099, https://doi.org/10.1175/JHM-D-15-0088.1.

Zrnic, D. S., and Coauthors, 2007: Agile-beam phased array radar for weather observations. *Bull. Amer. Meteor. Soc.*, **88**, 1753–1766, https://doi.org/10.1175/BAMS-88-11-1753.